ELSEVIER

Journal of Fluids and Structures 26 (2010) 979–993

JOURNAL OF FLUIDS AND STRUCTURES

www.elsevier.com/locate/jfs

An investigation into the effects of unsteady parameters on the aerodynamics of a low Reynolds number pitching airfoil

M.R. Amiralaei, H. Alighanbari*, S.M. Hashemi

Department of Aerospace Engineering, Ryerson University, Victoria Street, Toronto, Ontario, Canada M5B 2K3

Received 7 December 2009; accepted 13 June 2010
Available online 29 July 2010

Abstract

The growing applications of low Reynolds number (LRN) operating vehicles impose the need for accurate LRN flow solutions. These applications usually involve complex unsteady phenomena, which depend on the kinematics of the vehicle such as pitching, plunging, and flapping of a wing. The objective of the present study is to address the issues related to LRN aerodynamics of a harmonically pitching NACA0012 airfoil. To this end, the influence of unsteady parameters, namely, amplitude of oscillation, d, reduced frequency, k, and Reynolds number, Re, on the aerodynamic performance of the model is investigated. Computational fluid dynamics (CFD) is utilized to solve Navier–Stokes (N–S) equations discretized based on the Finite Volume Method (FVM). The resulting instantaneous lift coefficients are compared with analytical data from Theodorsen's method. The simulation results reveal that d, k, and Re are of great importance in the aerodynamic performance of the system, as they affect the maximum lift coefficients, hysteresis loops, strength, and number of the generated vortices within the harmonic motion, and the extent of the so-called figure-of-eight phenomenon region. Thus, achieving the optimum lift coefficients demands a careful selection of these parameters.

Keywords: Low Reynolds number; Pitching airfoil; Unsteady aerodynamics; CFD

1. Introduction

The emergence of micro-aerial and underwater vehicles has been the major reason for the surge in the recent research endeavours in the LRN fluid dynamics discipline. The successful design and modelling of these applications are quite demanding in terms of accurate flow field solutions, and strongly depend on the knowledge of flow patterns and structures. LRN flows are inherently complex, vastly unsteady, and mostly viscous. The occurrence of the respective viscous phenomena depends on numerous factors such as kinematics and the operating Re. Therefore, appropriate solution methods are necessary to obtain reasonably accurate results.

The underlying LRN lift generation mechanisms and the corresponding fluid phenomena: unsteady wing movements, dynamic stall, rotational effects, wake capturing, vortex interaction, and LE/TE vortices are well addressed in the studies of Dickinson and Götz (1993), Dickinson et al. (1999), McCroskey (1982), McCroskey and Pucci (1982), Sun and Tang (2002) and Weis-Fogh (1973). However, the details of the flow structures, influential flow and system

*Corresponding author. Tel.: +1 416 979 5000; fax: +1 416 979 5265.
E-mail address: halighan@ryerson.ca (H. Alighanbari).

0889-9746/$ - see front matter © 2010 Elsevier Ltd. All rights reserved.
doi:10.1016/j.jfluidstructs.2010.06.004

Nomenclature

b	half of the airfoil chord length ($b = c/2$)	Re	Reynolds number ($U_\infty c/\nu$)
c	airfoil chord length	T	period of oscillation
C_d	drag coefficient	t	physical time
$C_{d,max}$	maximum drag coefficient	TE	airfoil trailing edge
$C_{d,min}$	minimum drag coefficient	U_∞	freestream velocity
C_l	lift coefficient	u_i	component of velocity in i direction ($i = 1$ and 2)
$C_{l,max}$	maximum lift coefficient	x/c	pitching axis location
d	amplitude of oscillation	α	instantaneous angle of attack
f	frequency of oscillation	α_0	mean angle of attack
k	reduced frequency ($k = \pi fc/U_\infty$)	ν	kinematic viscosity
LE	airfoil leading edge	ρ	fluid density
p	static pressure	τ	nondimensional time (t/T)

parameters on the aerodynamics, and the effectiveness of each phenomenon at different conditions are not thoroughly understood. Hence, further investigations are required to obtain a better insight into these types of flows. Two-dimensional (2-D) LRN unsteady studies are extremely useful in understanding the flow characteristics and can assist in evaluating the dependence of the aerodynamic performance on different parameters such as the amplitude of oscillation, reduced frequency, Re, and kinematic patterns. These investigations are also of great importance in revealing the effectiveness of the 3-D aspects, such as tip vortices, spanwise flow, and vortex interactions. 2-D dynamic pitching oscillation is one of the prevalent unsteady conditions in LRN flows for which each of the above-mentioned phenomena could occur and affect the flow field noticeably.

Several researchers have investigated LRN flows by utilizing analytical, experimental or numerical approaches. The application of analytical techniques is restricted to special cases of extremely simplified flow conditions such as quasi-steady solution or Theodorsen's method for 2-D harmonic pitching and plunging oscillations [e.g., see Leishman (2006)]. Unfortunately, fewer studies are conducted on LRN pitching motions than those at intermediate and high Re, both experimentally and numerically. Experimental means yield the most reliable results, but these methods are highly expensive and time consuming. Jung and Park (2005) experimentally showed the strong dependence of a pitching airfoil vortex shedding on the reduced frequency, k. The experiments by Fuchiwaki and Tanaka (2006) on a pitching airfoil at $\mathrm{Re} = 4000$ showed the dependence of the shed vortices and their scales on k; however, they showed that these vortical structures are independent of the airfoil configuration and mean angle of attack, α_0. The influence of k on the dynamic lift coefficients is investigated in another study by Fuchiwaki et al. (1999). Koochesfahani (1989) conducted a series of LRN experiments and showed the strong dependence of the resulting wake structures and thrust coefficients of a pitching airfoil on frequency and amplitude of oscillation. In a similar study, the vortex–vortex interactions and their influence on the aerodynamic forces were explored by Shih et al. (1995).

Akbari and Price (2003) simulated the LRN flow field around a pitching airfoil utilizing N–S equations. They examined the effects of Re, k, α_0, and x/c on the predicted aerodynamic forces and concluded that k and Re have the maximum and minimum effects, respectively, amongst the investigated parameters. Jameson (1991) showed the importance of amplitude of oscillation and viscous terms by solving Euler equations. Yang et al. (2006) examined the impact of α_0 on fluid flow by simulating the compressible Euler equation based on FVM. Okong'o and Knight (1997) simulated 2-D, laminar, compressible flow using N–S equations with FVM for $\mathrm{Re} = 10^4$ and 2×10^4. They concluded that the main influence of increasing Re is to reduce the angle of attack at which the primary recirculation region starts to develop on the leeward side of the airfoil. They also showed that increasing Re causes the location of these recirculation regions to become closer to the LE of the model. Hamdani and Sun (2000) solved 2-D compressible N–S equations for the flow field of pitching and plunging motions at $\mathrm{Re} = 100$ and obtained large unsteady forces, attributed to extensive generated vortical patterns. Chandar and Damodaran (2008) numerically solved 2-D airfoil flow using moving overlapping grids for $\mathrm{Re} = 10^4$ and 4.5×10^4 and assumed laminar flow, which led to good agreement with experimental results. Young and Lai (2004) and Amiralaei et al. (2009) investigated the effects of frequency and amplitude of oscillations on the 2-D flow field of an airfoil, where Young and Lai (2004) showed that thrust coefficients are dependent on the product $k\alpha$ rather than k or α individually. Visbal and Shang (1989) conducted a 2-D numerical study over a pitching airfoil and concluded that the forces and induced vortical structures depend on pitch rate and pitching axis location (x/c). They also showed that the highly unsteady flow structures are accompanied by reverse flow

in the boundary layer, shedding of TE vortex into downstream, and formation of LE vortex with a shear layer on the leeward section of the airfoil.

The present study is geared towards gaining a better understanding of the effect of some unsteady parameters on the instantaneous lift and drag coefficients of a NACA0012 airfoil under harmonic pitching oscillations. These parameters are d, k, and Re and the study is conducted for the Re range of $555 \leq \mathrm{Re} \leq 5000$. CFD is the solution approach and 2-D N–S equations discretized based on FVM are the governing equations. The flow is assumed to be incompressible and laminar, and the simulation is performed in OpenFOAM (e.g. see the OpenFOAM user guide cited herein, 2008).

2. Theory and numerical simulations

2.1. Governing equations and flow solver

The governing equations for the laminar incompressible flow of a harmonically pitching NACA0012 airfoil are the 2-D N–S equations, which can be expressed in their indicial form as the following:

$$\frac{\partial u_i}{\partial x_i} = 0, \tag{1}$$

$$\frac{\partial u_i}{\partial t} + \frac{\partial u_i u_j}{\partial x_j} = -\frac{\partial p}{\partial x_i} + \frac{1}{\mathrm{Re}} \frac{\partial^2 u_i}{\partial x_j \partial x_j}, \tag{2}$$

where $i = 1$ and 2 represent the x and y coordinate, respectively, and u_i is the velocity in i direction.

These equations are discretized based on FVM in OpenFOAM (OpenFOAM user guide, 2008) and the desired pitching motion is implemented. Diffusive terms are considered due to their importance in LRN flows. The flow is assumed to be laminar and incompressible. The governing equations, which consist of continuity and momentum, are solved in a fixed reference frame, and Laplace smoothing mesh motion algorithm is used to handle the mesh motion.

In the present analysis, convective and diffusive terms are discretized based on a second order central differencing scheme, and the first order Euler implicit scheme is used for the transient terms. The resulting linear system of equations is treated with a preconditioned conjugate gradient (PCG) solver and the pressure–velocity coupling was obtained using a pressure implicit and splitting of operators (PISO) algorithm.

2.2. Mesh generation and boundary conditions

An O-type mesh is generated to model the airfoil and the surrounding flow. The selection of the O-type mesh over a C-type is based on an earlier study by Yang et al. (2006). They proved that the former mesh is computationally less expensive, but yields almost the same aerodynamic forces as those resulting from the latter. The schematic of the O-type grid used for the present simulations is shown in Fig. 1.

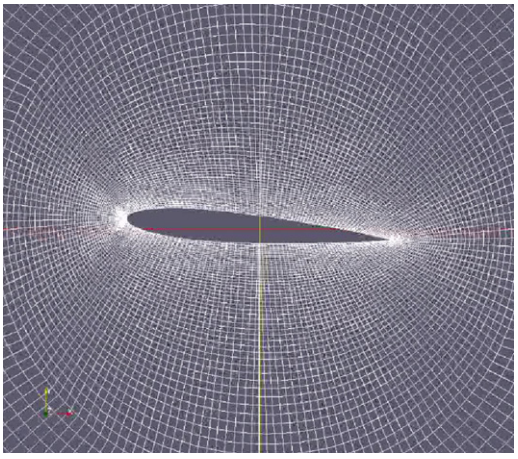

Fig. 1. Schematic of the O-type grid around the airfoil.

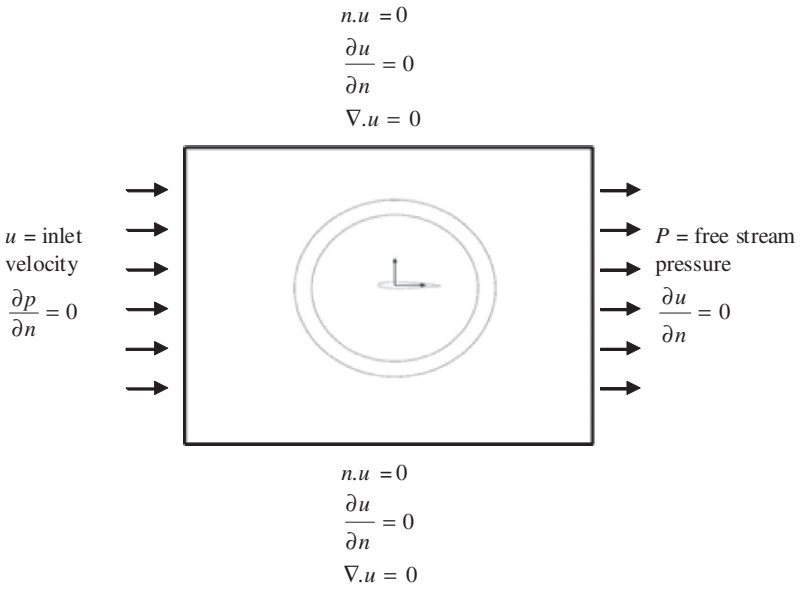

Fig. 2. Schematic of computational domain and the boundary conditions.

The continuity equation demands initial conditions on p, while momentum equations need the initial velocity components on u and v. The steady state solutions are used as the initial conditions for the time marching calculations. Along the airfoil surface a no-slip boundary condition is applied. The far-field boundary is set to $30c$ from the airfoil such that its effect on the flow surrounding the moving surface is negligible (see Lentink and Gerritsma, 2003; Boss et al., 2008) and is set to a slip boundary condition, as illustrated in Fig. 2. At the inflow boundary, the velocity is specified (velocity Dirichlet boundary condition) based on the desired Re, and the pressure is restricted to the zero-gradient condition. At the outflow boundary, the pressure is set to the freestream value, while the velocity is set to the zero-gradient condition. The present simulations are conducted for a mesh size of 26×10^3 and temporal resolution of 2000 time steps within one oscillation cycle.

2.3. Validation studies

In order to assess the accuracy of the results, extensive examinations are performed to address the issues concerning grid sensitivity and time step resolution. Also, several simulations are conducted and the results are compared with the existing database in the literature (Henderson, 1995; Williamson, 1995; Bos et al., 2008; Guilmineau and Queutey, 2002; Mahfouz and Badr, 2000; Okajima et al., 1975; Akbari and Price, 2003). The lift coefficients are also compared with those obtained from Theodorsen's method. This is done to show that Theodorsen's method only yields reasonable results when the effect of viscosity is minimal, and to show that the numerical simulations greatly differ from Theodorsen's results qualitatively as well as quantitatively, when significant viscosity and vortical structures exist.

Since the quality of the simulation results depends on the mesh and temporal resolution, a convergence study is first carried out to find the appropriate mesh size and time step for the present study. The pitching motion equation for the mesh dependence analysis is $\alpha = \alpha_0 + d\sin(2\pi ft)$. This grid analysis is performed for several cases; however, only the results for $d = 2^\circ$, Re = 555 and $d = 10^\circ$, Re = 5000 are presented here for the sake of brevity. Four different mesh sizes were considered: 5×10^3, 11×10^3, 26×10^3, and 50×10^3, corresponding to 100, 140, 176, and 200 points on the airfoil surface, respectively, and each simulation emerged from its fully converged stationary solution. The lift coefficients versus time were obtained for each case, and since they are small, the close view of their peak values is depicted in Fig. 3(a) and (b). The difference between the computed C_l with 26×10^3-cells and with 50×10^3-cells was found to be negligible. Thus, the mesh of 26×10^3-cells was selected as the baseline mesh for further analyses.

Similar observations are also made for the temporal resolution analysis. The baseline grid (26×10^3) was examined for several time steps: 500, 1000, 2000, and 4000, within one excitation period. As expected (see Ferziger and Peric, 1999) the results are less sensitive to the temporal resolution than the spatial refinement. The lift coefficients for 2000

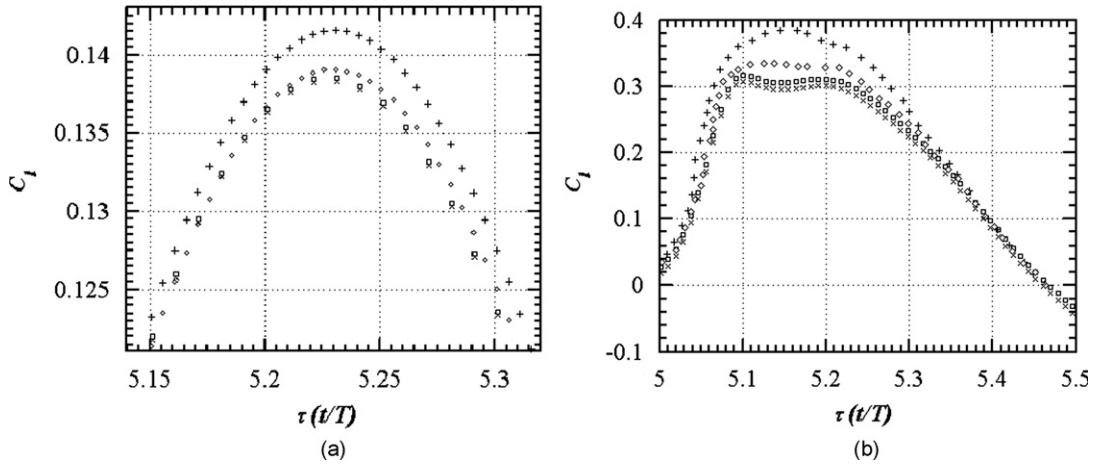

Fig. 3. Peak lift coefficients versus nondimensional time for different mesh sizes ($k = 0.1$, $x/c = 0.25$): +, 5×10^3; ◇, 11×10^3; □, 26×10^3; ×, 50×10^3, (a) $d = 2^\circ$ and $\mathrm{Re} = 555$; (b) $d = 10^\circ$ and $\mathrm{Re} = 5000$.

Table 1
Influence of different mesh sizes and temporal resolution, difference is calculated based on the baseline case (26×10^3 cells and 2000 time steps).

$T/\Delta t$	Grid size $\times 10^3$	Difference (%)
500	26	1.47
1000	26	1.0
4000	26	0.2
2000	5	2.6
2000	11	1.2
2000	50	0.4

and 4000 time steps had negligible differences (Table 1). Therefore, we conclude that with the present solver settings, 26×10^3 cells and 2000 time steps are sufficient and yield accurate results for the dynamic pitching simulations.

The simulations are further validated against the existing literature. First, the fluid flow of a stationary cylinder with $\mathrm{Re} = 150$ is simulated, which refers to a fully laminar flow (Henderson, 1995; Williamson, 1995; Bos et al., 2008). The calculated mean drag coefficient of the present simulation ($\overline{C}_\mathrm{d} = 1.375$) is in close agreement with that of Henderson (1995). Fig. 4 shows the computed drag coefficient.

Secondly, the vertical oscillation (plunging motion) of a cylinder at $\mathrm{Re} = 185$ is simulated. This case has been investigated by Bos et al. (2008) and Guilmineau and Queutey (2002). The motion is governed by $y(t) = -A_e \sin(2\pi f_e t)$, where $A_e = 0.2c$ and $f_e = 0.154$. The calculated mean drag coefficient is $\overline{C}_d = 1.25$, which matches the result of Bos et al. (2008), where $\overline{C}_d = 1.25$. The obtained $\overline{C}_d$ is also in close agreement with that of Guilmineau and Queutey (2002), where $\overline{C}_d = 1.2$. Fig. 5 shows the simulated drag coefficient, and the generated von Karman vortex in the downstream wake of the plunging cylinder in presented in Fig. 6.

The flow field of a pitching circular cylinder is also simulated following the studies by Mahfouz and Badr (2000) and Okajima et al. (1975). The nondimensional surface velocity of the cylinder is given by $U_w = 0.2 \sin(0.1\pi t)$, and $\mathrm{Re} = 40$. The calculated C_l is in good agreement with that of Mahfouz and Badr (2000) and Okajima et al. (1975), as shown in Fig. 7.

Moreover, the pitching oscillation of a NACA0012 airfoil studied by Akbari and Price (2003) is investigated. The pitching oscillation is governed by $\alpha = 15^\circ + 10^\circ \cos(2\pi f t)$, and $k = 0.25$ ($k = \pi f c/U_\infty$) and $\mathrm{Re} = 3000$. Fig. 8 shows the normal force coefficient (C_n) versus α, which is in close agreement with that of Akbari and Price (2003). The observed discrepancy could be related to the different LE/TE geometries considered for the NACA0012 models, or it could be due to the different utilized time and grid resolutions.

Finally, the lift coefficients obtained from this numerical study are compared with those calculated from Theodorsen's method. The details of Theodorsen's method are well documented [e.g., see Leishman (2006) and the

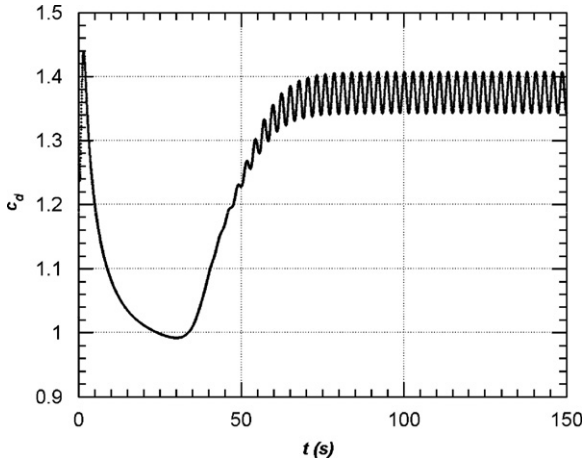

Fig. 4. Drag coefficient of a stationary cylinder at Re = 150.

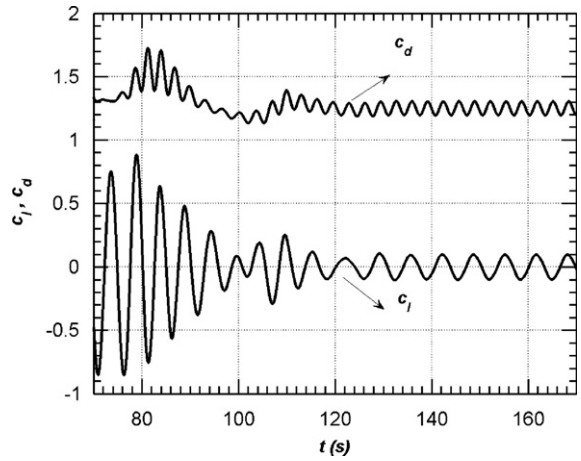

Fig. 5. Lift and drag coefficient of a plunging cylinder at Re = 185 ($y(t) = -A_e \sin(2\pi f_e t)$, where $A_e = 0.2c$ and $f_e = 0.154$).

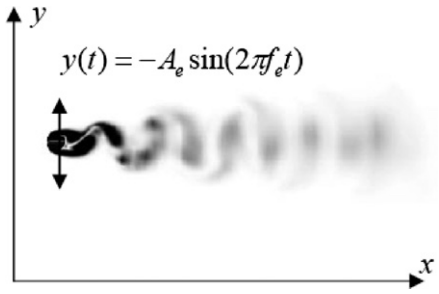

Fig. 6. Von Karman vortex street behind a plunging cylinder at Re = 185 where $A_e = 0.2c$ and $f_e = 0.154$.

references cited therein]; however, for the sake of completeness, a brief explanation is given here. Theodorsen's method for pitching airfoils is based on inviscid, incompressible, and small disturbance assumptions and yields the aerodynamic lift by the following equation:

$$L = \pi\rho V^2 b\left[\frac{b}{V}\dot{\alpha} - \frac{b^2}{V^2}a\ddot{\alpha}\right] + 2\pi\rho V^2 b\left[\alpha + \frac{b\dot{\alpha}}{V}\left(\frac{1}{2} - a\right)\right]C(k), \tag{3}$$

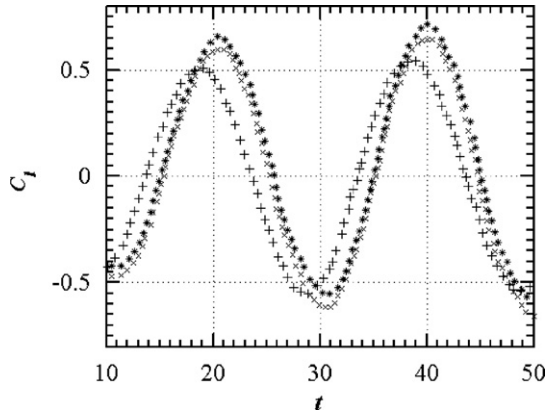

Fig. 7. Lift coefficient of a pitching cylinder at Re = 40, $U_w = 0.2\sin(0.1\pi t)$: +, Mahfouz and Badr (2000); ×, Okajima et al. (1975); ∗, present simulation.

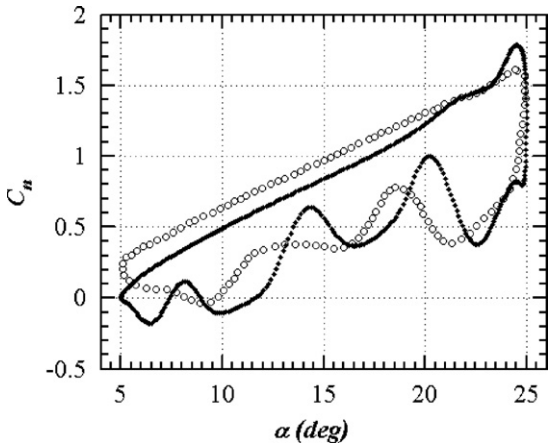

Fig. 8. Normal force coefficient (C_n) of a pitching NACA0012 at Re = 3000 ($\alpha = 15^\circ + 10^\circ\cos(2\pi ft)$, $k = .25$, where $k = \pi fc/U_\infty$): -, present simulation; o, Akbari and Price (2003).

where ρ, b, V, α, a, and $C(k)$ are, respectively, the density, airfoil half-chord length, flow velocity, instantaneous angle of attack, pitching axis location, and Theodorsen's function. For pure pitching oscillations ($\alpha = \bar{\alpha}\,e^{i\omega t}$) the lift coefficient ($C_l$) is obtained by the following equation:

$$C_l = 2\pi(F[1+ik] + G[i-k])\bar{\alpha}e^{i\omega t} + \pi k\left(i-\frac{k}{2}\right)\bar{\alpha}e^{i\omega t}, \tag{4}$$

where k is the reduced frequency, and F and G are the real and imaginary parts of Theodorsen's function ($C(k) = F(k)+iG(k)$), respectively.

In the present study, the pitching motion is governed by the following equation:

$$\alpha = \alpha_0 + d\sin(2\pi ft) \tag{5}$$

The simulation is conducted for both viscous and inviscid flow where Re = 555, $k = 0.1$, and $d = 2^\circ$. According to Leishman (2006), Theodorsen's method gives accurate results for small amplitudes of oscillation and reduced frequencies. Fig. 9 shows that our inviscid simulation matches the results of Theodorsen's method; however, for viscous flow, the numerically computed lift coefficients are slightly lower than those calculated from Theodorsen's method (Fig. 9).

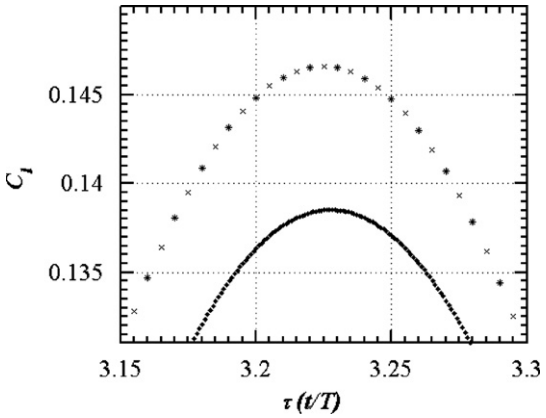

Fig. 9. Lift coefficient versus nondimensional time (Re = 555, $k = 0.1$, $d = 2°$): –, viscous N–S simulation; ×, inviscid N–S simulation; ∗, Theodorsen.

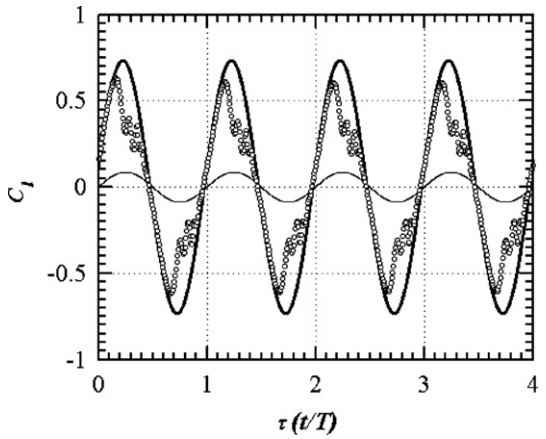

Fig. 10. Lift coefficient versus nondimensional time (Re = 555, $k = 0.1$, $d = 10°$): o, numerical; ▬, Theodorsen (airfoil pitch angle is also shown on the figure: —, $\alpha/2$).

Fig. 10 shows the lift coefficients versus nondimensional time for the aforementioned parameters. In this figure, the lift coefficient computed by the numerical solution of the viscous N–S equations is compared with that calculated via Theodorsen's method. Fig. 10 shows that the difference between the analytical and numerical results is increased for $d = 10°$, which can be related to the breakdown of Kutta condition (see Leishman, 2006) and the stronger effects of vortices around TE, which cause inaccuracies in the predictions of the analytical method.

3. Results and discussion

The present parametric study is carried out to investigate the influence of d, k, and Re on the aerodynamics of a NACA0012 where $x/c = 0.25$. A summary of the case-studies is shown in Fig. 11. The emphasis in this work is put on the influence of the abovementioned parameters on the generated lift and drag coefficients, and wherever necessary the vortical patterns around the model are discussed in detail.

3.1. Effects of amplitude of oscillation

The effect of the airfoil amplitude of oscillations on the simulated lift coefficients is first explored. The instantaneous C_l versus τ is depicted in Fig. 12 for $d = 2°$, $4°$, $6°$, $8°$, and $10°$, where $k = 0.1$ and Re = 555. As illustrated, the maximum

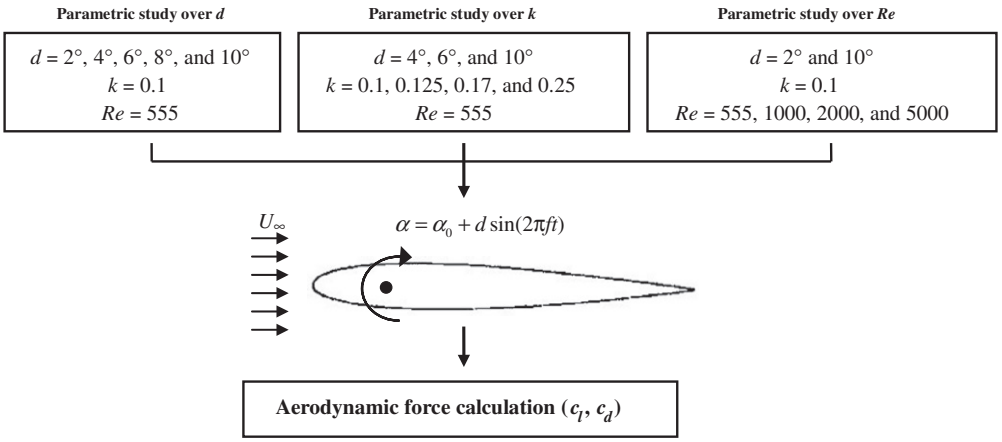

Fig. 11. Schematic view of the conducted case-studies.

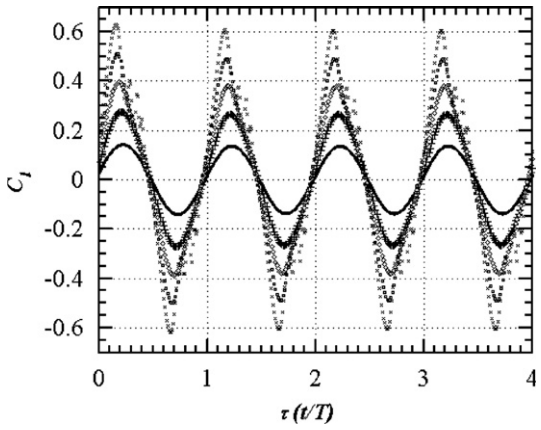

Fig. 12. Lift coefficient versus nondimensional time: -, $d=2^\circ$; +, $d=4^\circ$; ◇, $d=6^\circ$; □, $d=8^\circ$; ×, $d=10^\circ$.

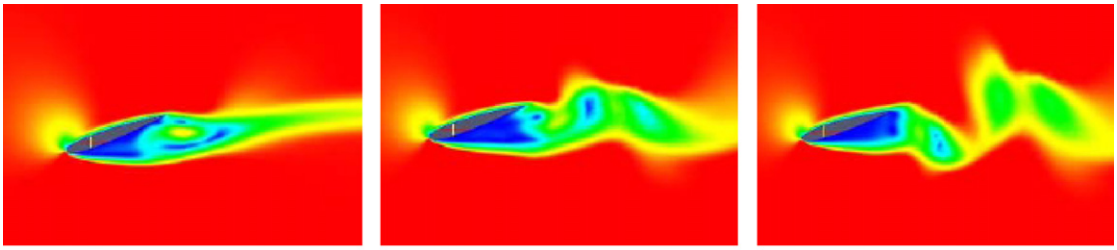

Fig. 13. The generated vortical structures after the peak C_l, $d=10^\circ$, $k=0.1$, Re = 555: (a) $\alpha=-9.75^\circ$; (b) $\alpha=-7.8^\circ$; (c) $\alpha=-5.6^\circ$.

lift coefficient ($C_{l,max}$) increases at higher amplitudes of oscillations. The calculated lift coefficients are periodic and harmonic; however, for $d=8^\circ$ there is a deviation from sinusoidal behaviour after the peak lift coefficient. This deviation is more noticeable in the $d=10^\circ$ case, which can be explained by the generation of three consecutive vortices at the TE of the airfoil. These counter-rotating vortical structures are shown in Fig. 13. Furthermore, increasing d induces significant lead in the C_l results meaning that $C_{l,max}$ is obtained at a lower τ (Fig. 12). This can be attributed to the stronger effects of shed wake and vortical structures on the surrounding fluid at higher amplitudes.

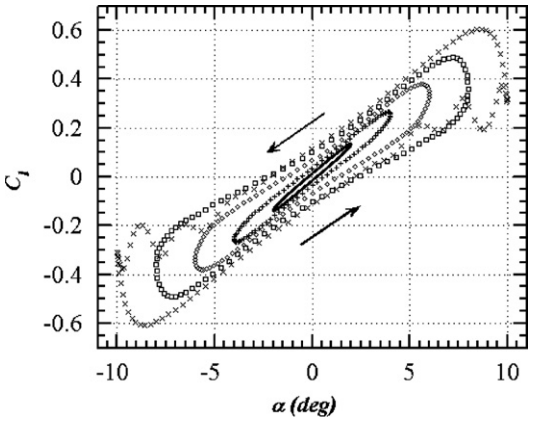

Fig. 14. Lift coefficient versus angle of attack ($k = 0.1$, Re = 555): -, $d = 2°$; +, $d = 4°$; ◇, $d = 6°$; □, $d = 8°$; ×, $d = 10°$.

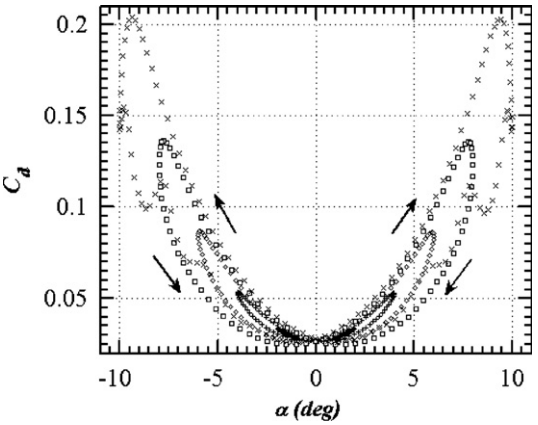

Fig. 15. Drag coefficient versus angle of attack ($k = 0.1$, Re = 555): -, $d = 2°$; +, $d = 4°$; ◇, $d = 6°$; □, $d = 8°$; ×, $d = 10°$.

Fig. 14 shows C_l versus α for the conducted simulations. As can be seen, the hysteresis loops are broadened for larger amplitudes. It means that at larger amplitudes, for the same angle of attack, the airfoil produces higher lift during downstroke than upstroke. The existence of these loops is the result of the induced velocities, which result in different lift coefficients between upstroke and downstroke. In addition, despite the influence of d on the maximum lift coefficient, hysteresis loop width, and lift enhancing vortical structures, it does not have a noticeable effect on the lift curve slopes (Fig. 14). The predicted drag coefficients versus angle of attack are illustrated in Fig. 15 showing a figure-of-eight pattern. Likewise the C_l curves (Fig. 14), the maximum value ($C_{d,max}$) as well as hysteresis loop width are increased at higher amplitudes of oscillations. The upstroke C_d is higher than the downstroke one, which is against the trend seen in Fig. 14. Also, $C_{d,min}$ is almost constant and does not change with d noticeably.

3.2. Effects of reduced frequency

The effect of reduced frequency on the unsteady pitching motion is investigated by plotting the C_l versus α curves for several reduced frequencies: $k = 0.1$, 0.125, 0.17, 0.25 at Re = 555 and $d = 4°$, 6°, and 10°. As shown in Fig. 16 ($d = 4°$), $C_{l,max}$ increases with reduced frequency; from $C_{l,max} = 0.265$ at $k = 0.1$ to $C_{l,max} = 0.27$ at $k = 0.125$ and from $C_{l,max} = 0.275$ at $k = 0.17$ to $C_{l,max} = 0.28$ at $k = 0.25$. Moreover, a higher k broadens the hysteresis loops, but does not have any noticeable effect on the lift curve slope. A similar behaviour is observed for $d = 6°$ (Fig. 17); however, in this case, k has a stronger effect on the lift coefficients and a more noticeable effect on $C_{l,max}$. That is, increasing k changes

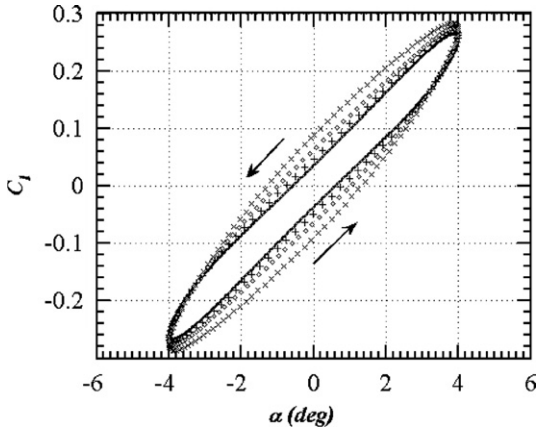

Fig. 16. Lift coefficient versus angle of attack ($d = 4°$, Re = 555): -, $k = 0.1$; +, $k = 0.125$; ◇, $k = 0.17$; ×, $k = 0.25$.

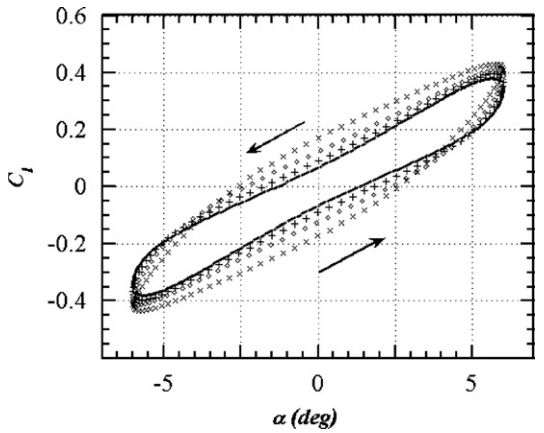

Fig. 17. Lift coefficient versus angle of attack ($d = 6°$, Re = 555): -, $k = 0.1$; +, $k = 0.125$; ◇, $k = 0.17$; ×, $k = 0.25$.

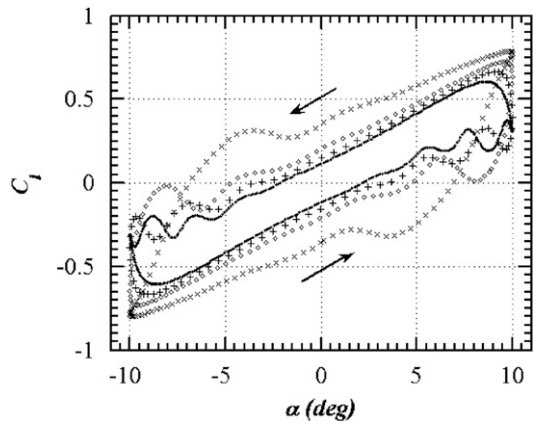

Fig. 18. Lift coefficient versus angle of attack ($d = 10°$, Re = 555): -, $k = 0.1$; +, $k = 0.125$; ◇, $k = 0.17$; ×, $k = 0.25$.

$C_{l,max}$ from 0.38 at $k = 0.1$ to $C_{l,max} = 0.4$ at $k = 0.125$ and from $C_{l,max} = 0.41$ at $k = 0.17$ to $C_{l,max} = 0.43$ at $k = 0.25$. Fig. 18 reveals that increasing k at $d = 10°$, where there are consecutive vortical patterns in the C_l curves, has considerable influence on the strength of these vortices and their initiation location during the harmonic motion.

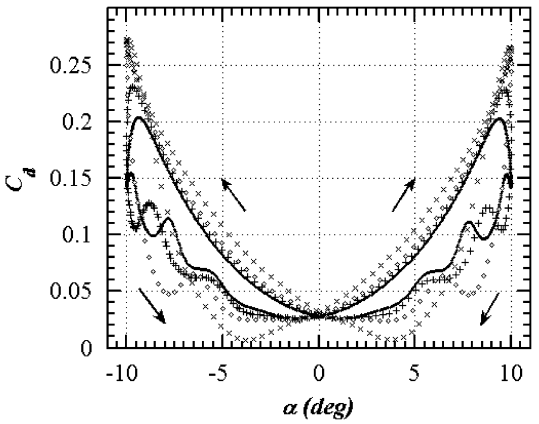

Fig. 19. Drag coefficient versus angle of attack ($d = 10^\circ$, Re = 555): -, $k = 0.1$; +, $k = 0.125$; ◇, $k = 0.17$; ×, $k = 0.25$.

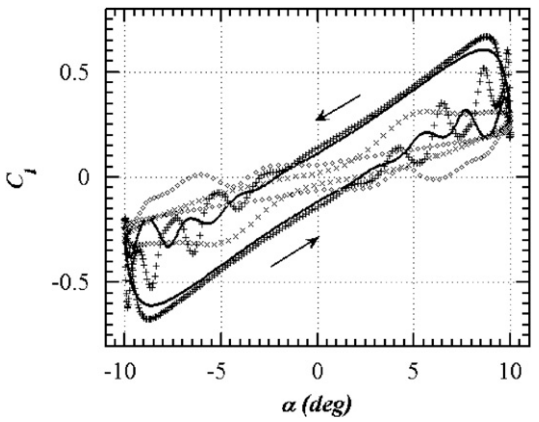

Fig. 20. Lift coefficient versus angle of attack ($d = 10^\circ$, $k = 0.1$): -, Re = 555; +, Re = 1000; ◇, Re = 2000; ×, Re = 5000.

As described in the previous section, three consecutive vortices are generated at TE after the peak value of lift for $k = 0.1$ and $d = 10^\circ$. These vortices amplify the lift force from the instant they are generated to the instant of their separation and shedding into the downstream wake. As k is increased to 0.125, the pitch angle at which these vortices form is changed from $\alpha = 10^\circ$ at $k = 0.1$ to $\alpha = 9.5^\circ$ at $k = 0.125$. The effect of these two vortices is observed at $k = 0.125$ (Fig. 18) in the lift coefficient curves, the second one occurring at $\alpha = 7^\circ$. At $k = 0.17$, the first vortex starts to develop and sheds at $\alpha \approx 8^\circ$. Moreover, as shown in Fig. 18, the number of effective vortices in the lift generation is reduced from three at $k = 0.1$ to two at $k = 0.125$ and to one at $k = 0.17$. The pitch angle of the first vortical structure is further changed to $\alpha \approx 4^\circ$ for $k = 0.25$, and this vortex is the only effective one in the simulated lift coefficients.

Fig. 19 shows the respective C_d versus α curve of Fig. 18. As shown, increasing the reduced frequency increases $C_{d,max}$ and broadens the hysteresis loop width. The effect of k during the downstroke is greater than during the upstroke. The minimum drag coefficient remains constant for $k = 0.1$, 0.125, and 0.17; however, it is reduced for $k = 0.25$, where the number of the vortical structures is reduced to one and occurs at $\alpha \approx 4^\circ$.

3.3. Effects of Reynolds number

The influence of Re on the simulated lift coefficients is studied for Re = 555, 1000, 2000, and 5000. This investigation is conducted for $k = 0.1$ and $d = 2^\circ$ and 10°, which are the lowest and highest considered amplitudes of oscillation in this study. As Re is increased from Re = 555 to 1000 for $d = 10^\circ$, the maximum lift coefficient increases from $C_{l,max} = 0.61$ to 0.67 (see Fig. 20); however, the pitch angle at which $C_{l,max}$ occurs remains the same, $\alpha \approx 9^\circ$ for both Re. The increase

in $C_{l,max}$ at Re = 1000 is accompanied by a figure-of-eight-phenomenon at $\alpha \approx 9.5^{\circ}$. After this point, the upstroke lift coefficients are higher than those at the downstroke at the same angle of attack. Both Re = 555 and 1000 include three sudden rise-and-falls after the peak lift coefficients. This behaviour can be attributed to the generation of extensive vortical patterns after the maximum angle of attack. Further increase in Re, Re = 2000, results in decrease in $C_{l,max}$ and decrease in the figure-of-eight phenomenon region. However, further increase of Re to 5000 slightly increases $C_{l,max}$ and eliminates the figure-of-eight phenomenon. Fig. 21(a)–(d) show the vortical patterns around the airfoil when $C_{l,max}$ is achieved. As can be seen, increasing Re from 555 to 1000 slightly increases the size of the TE vortex and the strength of the lower surface vortex. Further increase of Re from 1000 to 2000 causes the lower surface vortex to separate, which

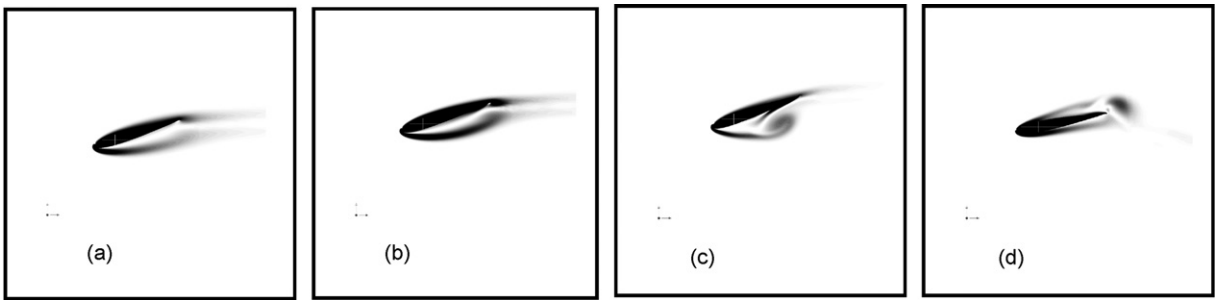

Fig. 21. Vortical patterns around the airfoil when $C_{l,\max}$ is obtained ($d = 10^{\circ}$, $k = 0.1$).

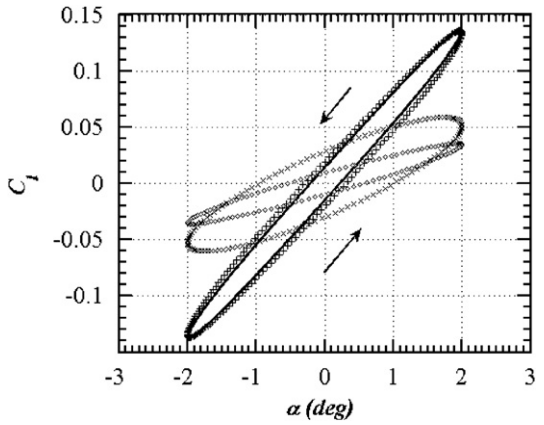

Fig. 22. Lift coefficient versus angle of attack ($d = 2^{\circ}$, $k = 0.1$): -, Re = 555; +, Re = 1000; ◇, Re = 2000; ×, Re = 5000.

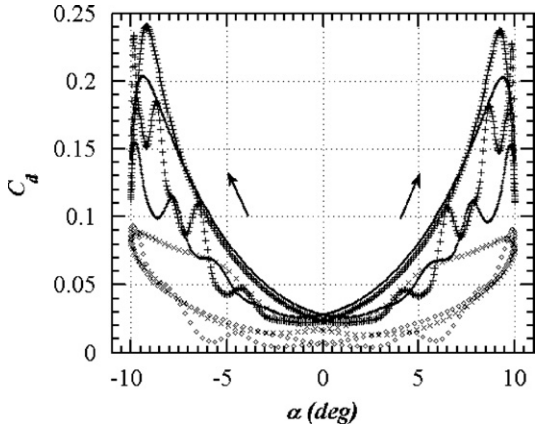

Fig. 23. Drag coefficient versus angle of attack ($d = 10^{\circ}$, $k = 0.1$): -, Re = 555; +, Re = 1000; ◇, Re = 2000; ×, Re = 5000.

could be the reason for the decrease of $C_{l,max}$ previously observed in Fig. 20. The lower and upper surface vortices are not separated from the airfoil at Re = 5000, but the TE vortex is separated and convected into the downstream wake. This could be the reason for higher $C_{l,max}$ at Re = 5000 than that Re = 2000, and the reason for lower $C_{l,max}$ than those at Re = 555 and 1000. The effect of increasing Re is also investigated at the lowest explored amplitude of oscillations, $d = 2^\circ$, and the same trends as those effects of Re at $d = 10^\circ$ are observed (see Fig. 22). Fig. 23 shows the C_d versus α curves at $d = 10^\circ$ for different Reynolds numbers. As can be seen, $C_{d,min}$ is reduced by increasing Re from 555 to 2000, but increases for Re = 5000.

4. Conclusion

A numerical aerodynamics study was carried out for a 2-D flow around a NACA0012 airfoil performing dynamic pitching motion in LRN regime. The aerodynamic characteristics of the model were explored and the effect of some unsteady flow and system parameters (d, k, and Re) on the instantaneous force coefficients and flow patterns were investigated. The analysis was conducted by means of Navier–Stokes equations discretized based on a finite volume approach. The results show the substantial influence of the aforementioned unsteady parameters on the maximum lift and drag coefficients. The parameters increase or decrease the aerodynamic force peak values depending on the surrounding flow structure. Hysteresis loops are also broadened or narrowed due to similar reasons. d and k do not have a noticeable effect on the lift curve slopes. It is also observed that d, k and Re are effective in changing the number, strength, and even the development angle of the generated vortical patterns. Moreover, a pattern called ''figure-of-eight phenomenon'' is observed in the predicted force coefficients at Re = 2000, which is eliminated at Re = 5000. Similar effects are noticed in the drag coefficient results, but the minimum drag coefficient is not affected substantially by the investigated parameters except at the high amplitudes of oscillation and high Reynolds numbers.

Acknowledgments

The authors gratefully acknowledge the financial support of the Natural Sciences and Engineering Council of Canada (NSERC) and Ryerson University.

References

Akbari, M.H., Price, S.J., 2003. Simulation of dynamic stall for a NACA 0012 airfoil using a vortex method. Journal of Fluids and Structures 17, 855–874.

Amiralaei, M.R., Alighanbari, H., Hashemi, S.M., 2009. Influence of unsteady parameters on the aerodynamics of a low Reynolds number pitching airfoil. In: Proceedings of the ASME 2009 International Mechanical Engineering Congress & Exposition IMECE2009, Lake Buena Vista, Florida, USA.

Bos, F.M., Lentink, D., Van Oudheusden, B.W., Bijl, H., 2008. Influence of wing kinematics on aerodynamic performance in hovering insect flight. Journal of Fluid Mechanics 594, 341–368.

Chandar, D.D.J., Damodaran, M., 2008. Computational study of unsteady low-Reynolds-number airfoil aerodynamics using moving overlapping meshes. AIAA Journal 46, 429–438.

Dickinson, M.H., Götz, K.G., 1993. Unsteady aerodynamic performance of model wings at low Reynolds numbers. The Journal of Experimental Biology 174, 45–64.

Dickinson, M.H., Lehman, F.O., Sane, S.P., 1999. Wing rotation and the aerodynamic basis of insect flight. Science 284, 1954–1960.

Ferziger, J.H., Peric, M., 1999. Computational Methods for Fluid Dynamics, 2nd ed Springer Verlag, Berlin.

Fuchiwaki, M., Tanaka, K., Tanaka, H., Kamemoto, K., Baysal, O., 1999. Flow patterns behind pitching airfoil and unsteady fluid forces. In: Proceedings of the 3rd ASME/JSME Joint Fluids Engineering Conference, San Francisco, CA, USA.

Fuchiwaki, M., Tanaka, K., 2006. Vortex structure and scale on an unsteady airfoil. JSME International Journal 49, 1056–1063.

Guilmineau, E., Queutey, P., 2002. A numerical simulation of vortex shedding from an oscillating circular cylinder. Journal of Fluids and Structures 16, 773–794.

Hamdani, H., Sun, M., 2000. Aerodynamic forces and flow structures of an airfoil in some unsteady motions at small Reynolds number. Acta Mechanica 145, 173–187.

Henderson, R.D., 1995. Details of the drag curve near the onset of vortex shedding. Physics of Fluids **7**, 2102–2104.

Jameson, A., 1991. Time dependent calculations using multigrid, with applications to unsteady flows past airfoils and wings. In: Proceedings of the AIAA 10th Computational Fluid Dynamics Conference, Honolulu, Hawaii, USA.

Jung, Y.W., Park, S.O., 2005. Vortex-shedding characteristics in the wake of an oscillating airfoil at low Reynolds number. Journal of Fluids and Structures 20, 451–464.

Koochesfahani, M.M., 1989. Vortical patterns in the wake of an oscillating airfoil. AIAA Journal 27, 1200–1205.
Leishman, J.G., 2006. Principles of Helicopter Aerodynamics, 2nd ed Cambridge University Press, London.
Lentink, D., Gerritsma, M., 2003. Influence of airfoil shape on performance in insect flight. In: Proceedings of the 33rd AIAA Fluid Dynamics Conference and Exhibit, Orlando, FL, USA.
Mahfouz, F.M., Badr, H.M., 2000. Flow structure in the wake of a rotationally oscillating cylinder. ASME Journal of Fluids Engineering 122, 290–301.
McCroskey, W.J., 1982. Unsteady airfoils. Annual Review of Fluid Mechanics 14, 285–311.
McCroskey, W.J., Pucci, S.L., 1982. Viscous–inviscid interaction on oscillating airfoils in subsonic flow. AIAA Journal 20, 167–174.
Okajima, O., Takata, H., Asanuma, T., 1975. Viscous flow around a rotationally oscillating circular cylinder. Institute of Space and Aeronautical Science Report 532, University of Tokyo.
Okong'o, N., Knight, D.D., 1997. Implicit unstructured Navier–Stokes simulation of leading edge separation over a pitching airfoil. In: Proceedings of the 35th AIAA Aerospace Sciences Meeting and Exhibit, Reno, NV, USA.
OpenFOAM, 2008. The Open Source CFD Toolbox User Guide, Version 1.5. OpenCFD Limited.
Shih, C., Lourenco, L.M., Krothapalli, A., 1995. Investigation of flow at leading edges of pitching—up airfoil. AIAA Journal 33, 1369–1376.
Sun, M., Tang, J., 2002. Lift and power requirements of hovering flight in *Drosophila virilis*. The Journal of Experimental Biology 205, 2413–2427.
Visbal, M.R., Shang, J.S., 1989. Investigation of the flow structure around a rapidly pitching airfoil. AIAA Journal 27, 1044–1051.
Weis-Fogh, T., 1973. Quick estimates of flight fitness in hovering animals, including novel mechanisms for lift production. The Journal of Experimental Biology 59, 169–230.
Williamson, C.H.K., 1995. Vortex dynamics in the wake of a cylinder. In: Green, S.I. (Ed.), Fluid Vortices. Fluid Mechanics and its Applications. Kluwer Academic Publishing, Dordrecht (Chapter 5).
Yang, S., Luo, S., Liu, F., Tsai, H.M., 2006. Subsonic flow over unstalled pitching airfoil computed by Euler method. In: 36th AIAA Fluid Dynamics Conference and Exhibit, San Francisco, CA, USA.
Young, J., Lai, J.C.S., 2004. Oscillation frequency and amplitude effects on the wake of a plunging airfoil. AIAA Journal 42, 2042–2052.